Annual performance and dynamic characteristics of a hybrid wind-wave floating energy system at a localized site in the North Sea

Zhou, Binzhen
School of Civil Engineering and Transportation, South China University of Technology

Zheng, Zhi
School of Civil Engineering and Transportation, South China University of Technology

Hu, Jianjian
School of Civil Engineering and Transportation, South China University of Technology

Lin, Chusen
School of Civil Engineering and Transportation, South China University of Technology

他

https://hdl.handle.net/2324/6790283

出版情報：Ocean Engineering. 280, pp.114872-, 2023-07-15. Elsevier
バージョン：
権利関係：

Annual performance and dynamic characteristics of a hybrid wind-wave floating energy system at a localized site in the North Sea

Binzhen Zhou[a], Zhi Zheng[a], Jianjian Hu[a], Chusen Lin[a], Peng Jin[b,*], Lei Wang[a], Yingyi Liu[c]

[a] *School of Civil Engineering and Transportation, South China University of Technology, Guangzhou 510641, China*

[b] *School of Marine Science and Engineering, South China University of Technology, Guangzhou 511442, China*

[c] *Research Institute for Applied Mechanics, Kyushu University, Kasuga, 816-8580, Japan*

Abstract

A hybrid system consisting of a spar-type wind turbine and an annular wave energy converter (WEC) is prospective in joint offshore wind-wave energy exploitation. Its coupled dynamic and power features in vast operating sea states are a valuable reference for design but are poorly understood. This study aims to fill the gap. By combining the wind module of OpenFAST and an in-house code, a numerical tool that can tackle the full aero-servo-hydro-mooring couplings in the hybrid system is developed. Dynamic features, mooring tensions, and energy conversion performance of a Hywind-annular WEC hybrid system are analyzed in a wide range of operating conditions with varying speeds of steady winds and periods of regular waves, emphasizing the effect of the annular WEC on the dynamic and power performance of the Hywind. Results show that the annular WEC improves the wind power generation below the rated wind speed and the stability of the Hywind by reducing its pitch displacement. But it also increases the motion amplitude in the heave direction. The annular WEC has a neglectable influence on the maximum mooring tensions. An evaluation of the annual wind-wave power based on hindcast sea states shows that wave power can effectively supplement wind power.

Keywords: spar-type floating wind turbine, wave energy converter, hybrid system, dynamic feature, energy conversion performance

1. Introduction

Joint exploitation of marine renewable energy from different sources is regarded as a sufficient use of the resource in a sea territory and has recently become an active research area [1]-[3]. Combined offshore wind-wave energy extraction is one of the prospective scenarios, as high winds and waves often coexist [4][5]. In the European Commission's Seventh Framework Programme (EU FP7) [6], renewable energy was emphatically planned in the branch theme Energy, Specific Programme "Cooperation", and supported by several coordinated projects to bring marine renewable energy closer to commercial use. The ORECCA (Offshore Renewable Energy Conversion Platform Coordination Action) Project [7]

* Corresponding author

E-mail address: jinpeng@scut.edu.cn (P. Jin)

focused on the challenges and developments in three recommended marine renewable energy sectors in deep seas (including wind, wave, and tidal steam) and the synergies and commonalities between them. The MARINA Platform project (Marine Renewable Integrated Application Platform) [8] aimed to develop new combined offshore wind and ocean energy concepts and new methods and new tools to evaluate their performance. It was the first EU-supported research to study integrated marine renewable energy systems, which significantly extended the ORECCA project. Inspired by projects like ORECCA and MARINA and subsidies and funds for similar efforts, a wide range of innovative concepts of hybrid wind-wave energy systems [9]-[13] based on different types of offshore wind turbines [14][15] and wave energy converters (WECs) [16][17] have been proposed.

Among the various hybrid wind-wave systems, the ones with a simple coaxial-cylinder configuration consisting of a spar-type floating wind turbine and an annular oscillating body WEC are extensively investigated [18]-[25]. The annular WEC is installed on the column of the spar foundation like a sleeve outside a shaft [26]. The annular WEC slides along the spar and generates wave power through a linear permanent magnet generator [27] power take-off (PTO) driven by the relative heave motion between the WEC and the spar. The configuration of such a hybrid system needs to be optimized to harness the maximum wave power [28]. Wan *et al*. [18] compared three configurations with a long spar, a short spar, and a shorter monopile. They found that the one with a long spar and large PTO damping has the best energy conversion performance. The use of control is also an important means to improve the efficiency of a wind-wave hybrid system and its adaptability in different wave conditions [29][30].

In practice, however, the properties of existing wind turbines are fixed and cannot be casually modified. The geometry and the PTO of the annular WEC are, therefore, deterministic to the energy conversion performance of the hybrid system. In most previous studies, the configuration of the annular WEC was directly brought from the Wavebob device [31], and the PTO damping was assigned randomly chosen, unoptimized values [19]. Till recently, a study by the authors systematically optimized the dimensions and PTO damping of the annular WEC in a hybrid system based on the OC3 Hywind wind platform [32]. The dynamic behaviours of the hybrid systems are also important indices that need to be revealed and calibrated in the pre-commercial stage [33][34]. Previous investigations of these issues were extensively carried out under the so-called "survival mode" [24] in extreme sea states. For example, Wan *et al*. [20] compared two survival modes where the annular WEC was respectively fixed on the spar at the mean water level (MWL mode) and submerged (SUB) mode. They found that under the SUB mode, the wave loads can be significantly reduced due to the avoidance of wave slamming. Wan *et al*. [21] investigated strong nonlinear phenomena, including the wave entry and exit and green water on deck, of a Hywind-annular WEC hybrid system. They showed that the green water on the deck even had a positive effect in reducing the motion response of the hybrid system.

As equipment includes disciplines of aerodynamics, control, and hydrodynamics, the hybrid wind-wave system can hardly be well simulated by traditional software or code of only wind turbines or floating body hydrodynamics. An integrated toolkit must be applied, at least in the present stage. The integrated toolkit commonly includes an aero-servo part, a hydrodynamic part, and a tool that can bridge the two by conveying information about motions and forces. Muliawan *et al*. [19] used a SIMO-TDHMILL3D combination and used empirical formulas to calculate the wind loads. Yde *et al*. [35] used a HAWC2-WAMSIM combination. Si *et al*. [11] and Ren *et al*. [36] used ANSYS/AQWA to simulate the hydrodynamics. The wind loads were simplified as a sum of thrust force and torque through empirical formulas and implemented by the user-defined function in ANSYS/AQWA. Wan *et al*. [18], Karimirad and Koushan [37], Michailides *et al*. [38], and Gao *et al*. [39] applied a SIMO-RIFLEX-AeroDyn combination. Their time-domain model employed a flexible joint to simulate the relative rotation between the main shaft and the tower. It implemented the one-way delivery of the loads on the rotor and nacelle to the tower. Wan *et al*. [20] used a Sesam-Wadam-SIMO combination for the frequency-domain and time-domain simulations. The tool for the wind turbine was not given explicitly.

From the literature, the previous studies of the spar-type wind turbine-annular WEC hybrid system emphasized dynamic responses and survivability in extreme waves. Under such situations, the annular WEC is fixed on the spar, and the interactions between them cannot be revealed. The dynamic features and wind-wave energy conversion performance of the hybrid system under operating conditions are also essential but relatively rarely investigated. Most of these studies [19][25][33][34] were carried out in sparse wind and wave conditions, where the wave parameters were determined by the wind parameters through empirical formulas [40]. A thorough analysis of the principles of dynamic and power performance in a wide range of wind and wave conditions is important for the designers but absent. In terms of the current numerical tools, most of them cannot tackle the full couplings between different parts in the hybrid system. For example, the SIMO-RIFLEX-AeroDyn combination fails to consider the delivery of the motion of the floating bodies to the servo of the turbine. The ANSYS/AQWA and user-force function combination assumes constant wind force and torque. The widely used OpenFAST is powerful in simulating wind turbines but cannot simulate multi-body hydrodynamics. While only part couplings are considered, the simulation leaves uncertainty and inaccuracy in the results.

This study aims to fill the gaps and its novelties are as follows: First, based on the systematically optimized Hywind-annular WEC hybrid system in a recent work of the authors [41], the previously overlooked coupled dynamic feature and power performance of the hybrid system in a wide range of wind and wave conditions are revealed, with an emphasis on the influence of the annular WEC on the dynamic and power performance of the Hywind. Second, this analysis involves couplings between the Hywind, the annular WEC, and the mooring, which, to the best of the authors' knowledge, were not well treated by existing tools. A numerical tool is proposed to handle the couplings, wherein an in-house code is developed to bridge the simulations of aerodynamics, hydrodynamics, and mooring.

The rest of the paper is organized as follows. In Section 2, the configuration and key parameters of the Hywind-annular WEC hybrid system are given. In Section 3, the theory behind the in-house code is provided and validated. In Section 4, the dynamic features, mooring tensions, and power performance of the hybrid system are analyzed and compared with an isolated Hywind. An evaluation of the annual mean power is also done based on hindcast sea states. In Section 5, the findings are concluded.

2. Configuration of the hybrid system

The wind-wave hybrid system consisting of a Hywind spar-type floating offshore wind turbine and an annular oscillating body WEC is shown in Figure 1. The WEC is assumed to be restricted and can only slide along the column of the spar. A linear permanent magnet generator [27] is installed between the spar and the WEC as the power take-off (PTO). Wave power is generated through the relative heave motion between the wind turbine and the WEC.

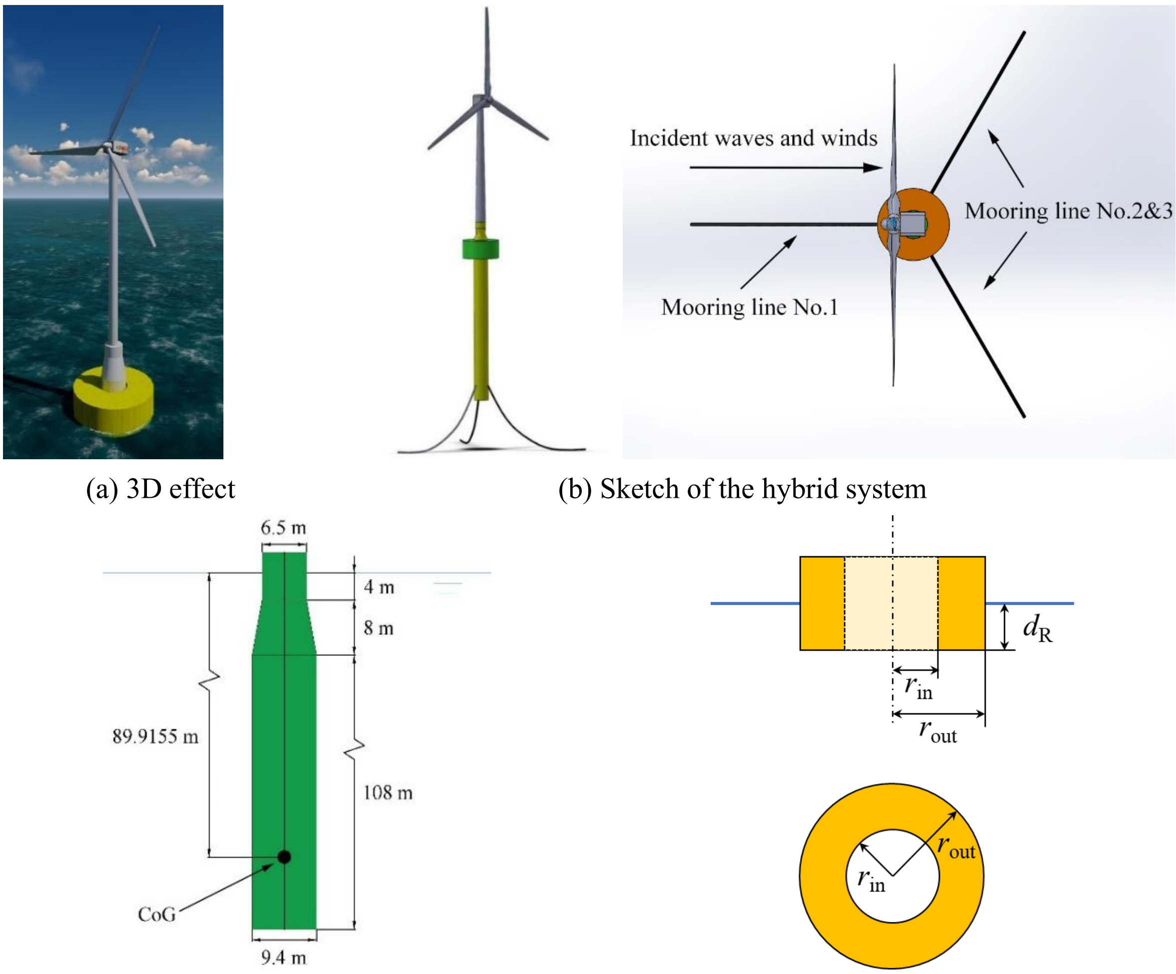

(a) 3D effect

(b) Sketch of the hybrid system

(c) Underwater part of the spar

(d) Sketch of the annular WEC

Figure 1 Layout of the Hywind-annular WEC hybrid system

2.1 *Hywind*

The OC3 Hywind [32] floating offshore wind turbine comprises the spar-type platform, the NREL 5 MW wind turbine, and the three-cable catenary mooring. The dimensions and inertia of the spar are given in Table 1. The key parameters of the NREL 5 MW wind turbine are shown in Table 2. The layout and properties of the mooring cables are presented in Figure 1b and Table 3, respectively. The data are from ref. [32].

Table 1 Parameters of the OC3 Hywind platform

Item	Value	Unit
Draft	120	m
Depth to top of taper below SWL	4	m
Depth to bottom of taper below SWL	12	m
Diameter above the taper	6.5	m
Diameter below the taper	9.4	m
Total mass (wind turbine included)	7,466,330	kg
Centre of gravity regarding SWL	−89.9155	m
Longitudinal moment of inertia	4,229,230,000	$kg \cdot m^2$
Transverse moment of inertia	4,229,230,000	$kg \cdot m^2$
Moment of inertia about the central axis	164,230,000	$kg \cdot m^2$

Table 2 Parameters of the NREL 5MW wind turbine

Item	Value and unit
Rated power	5 MW
Configuration	3 blades
Rotor diameter, Hub diameter	120 m, 3 m
Hub height	90 m
Cut-in, rated, cut-out wind speed	3 m/s, 11.4 m/s, 25 m/s
Shaft Tilt	5°
Rotor, nacelle, tower mass	110000 kg, 240000 kg, 347460 kg
Top diameter, base diameter	3.8 m, 6.0 m
Coordinates of the centre of gravity	(−0.2 m, 0.0 m, 64 m)

Table 3 Parameters of the mooring cables

Item	Value and unit
Number of Mooring Lines	3
Angle Between Adjacent Lines	120°
Depth to Anchors Below SWL	320 m
Radius to Anchors from Platform Centerline	853.87 m
Radius to Fairleads from Platform Centerline	5.2 m
Equivalent Mooring Line Mass Density	77.71 kg/m
Diameter of Mooring lines	9 cm
Unstretched Mooring Line Length	902.2 m
Equivalent Mooring Line Extensional Stiffness	3.84E+08 N/m

2.2 Annular WEC

The geometry of the annular WEC is characterized by its draft d_{WEC}, outer radius r_{out}, and inner radius r_{in}. The PTO of a linear generator is simplified and idealized as a linear damping [27]. The dimensions and PTO of the annular WEC have been optimized in our previous work [41] based on the wave condition in a target operation site at 59N3E in the North Sea [44] and are therefore employed in the present analysis. The optimized parameters are shown in Table 4 (b_{opt} being the optimal PTO damping).

Table 4 Parameters of the optimal annular WEC [41]

d_{WEC} (m)	r_{in} (m)	r_{out} (m)	Mass (kg)	b_{opt} (N·s/m)
1	5	20	1178.1	7.58×10^{6}

3. Modelling of the hybrid system

The full aero-hydro-servo couplings in the hybrid system are included in the present model, and its framework is shown in Figure 2. The wind turbine is simulated by the aero-servo module of OpenFAST. The coupled frequency-domain hydrodynamic coefficients of the floats, including added mass, radiation damping, and wave excitation force, are calculated by the WAFDUT code developed by the Dalian University of Technology based on a Higher Order Boundary Element Method (HOBEM) [48]. The mooring loads are calculated based on the catenary theory. All three tools are compiled by Fortran language. An in-house code also compiled by Fortran is developed to create interfaces to bridge the three. The in-house code also simulates the multi-body constraint dynamics, performs the frequency-to-time domain transformation of the multi-body motion equation, and calculates the wave power. The wind power is calculated by OpenFAST. The aerodynamic loads on the blades, nacelle, and tower are calculated by OpenFAST according to the wind speed and position of the turbine and are delivered by the in-house code to calculate the motion of the platform. The displacement and velocity of the platform are in turn delivered by the in-house code to the turbine. The mooring loads are calculated according to the motion of the platform and delivered by the in-house code to the platform. This numerical tool is developed because this analysis involves couplings between the Hywind, the annular WEC, and the mooring, which were not fully handled by previous tools (Table 5).

As the Blade Element Method (BEM) employed in OpenFAST and the Catenary Theory of mooring can be readily referred to in literature [45][46], they are not introduced here. An emphasis is on the time-domain equation of constrained dynamics of the two floats and the equations of wave power generation.

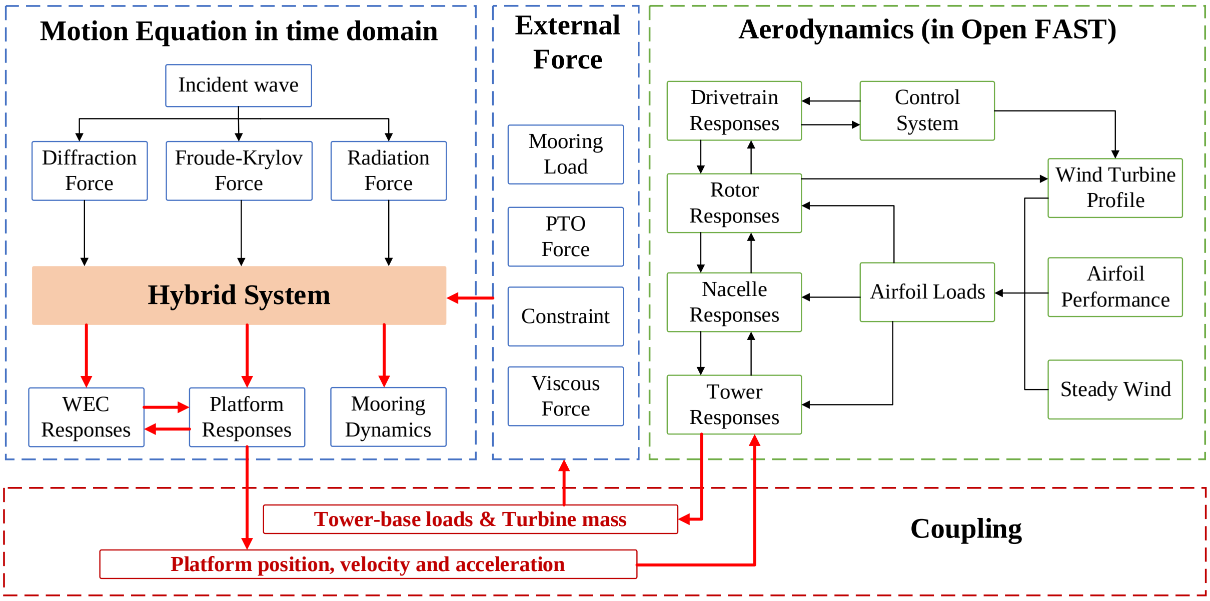

Figure 2 Coupling framework of the present numerical model

Table 5 Features of example previous numerical tools for wind-wave hybrid systems

Numerical tools	Features
SIMO-TDHMILL3D ANSYS/AQWA	Empirical formulas are used. The motion of the platform is not involved in the calculation of wind force and power.
SIMO-RIFLEX-AeroDyn	One-way delivery of the loads on the rotor and nacelle to the tower.
Sesam-Wadam-SIMO	The turbine simulation tool is not given explicitly.
HAWC2-WAMSIM	Multi-body constraint dynamics are not involved.

3.1 Constrained dynamics

The Hywind can move in six degrees of freedom (6 DoFs) under wind, wave, and mooring loads. The annular WEC is restricted and can only slide along the spar. The multi-DoF time-domain constrained dynamic equation of the hybrid system can be formulated based on Cummins' equation [47]:

$$\left[\mathbf{M}+\mathbf{a}_{\infty}\right]\ddot{\mathbf{X}}(t)+\int_{-\infty}^{t}\boldsymbol{\kappa}(t-\tau)\dot{\mathbf{X}}(\tau)d\tau+\mathbf{k}_{\mathrm{r}}\mathbf{X}(t)=\mathbf{F}_{\mathrm{ex}}(\mathbf{X},t)+\mathbf{F}_{\mathrm{c}}(t) \tag{1}$$

where $\mathbf{M}$ and $\mathbf{a}_\infty$ are the matrices of inertia and added mass for infinite wave frequency ($\omega \to \infty$), respectively. $\mathbf{k}_\mathrm{r}$ is the matrix of hydrostatic restoration coefficients. The inertia and hydrodynamic coefficients (added mass, radiation damping, and wave excitation force) of the floats are calculated using the WAFDUT. t and τ are the terms associated with time. $\mathbf{X}(t)$, $\dot{\mathbf{X}}(t)$, and $\ddot{\mathbf{X}}(t)$ are the vectors of displacement, velocity, and acceleration, respectively. $\boldsymbol{\kappa}(t-\tau)$ is the matrix of radiation impulse response function, which can be calculated using a refined Filon quadrature method proposed by Liu [49]. $\mathbf{F}_\mathrm{c}(t)$ is the constraint force. $\mathbf{F}_\mathrm{ex}(t)$ is the sum of the time-dependent external forces:

$$\mathbf{F}_\mathrm{ex}(t) = \mathbf{F}_\mathrm{wave}(t) + \mathbf{F}_\mathrm{PTO}(t) + \mathbf{F}_\mathrm{wind}(\mathbf{X}, t) + \mathbf{F}_\mathrm{moor}(\mathbf{X}, t) + \mathbf{F}_\mathrm{vis}(t) \tag{2}$$

where $\mathbf{F}_\mathrm{wave}(t)$, $\mathbf{F}_\mathrm{PTO}(t)$, $\mathbf{F}_\mathrm{wind}(t)$, $\mathbf{F}_\mathrm{moor}(t)$, and $\mathbf{F}_\mathrm{vis}(t)$ are the wave excitation force, PTO force, wind force, mooring tension, and fluid viscous force, respectively. The wind force and mooring tension are calculated by the aero-servo module of OpenFAST and the Catenary Theory, respectively. The fluid viscous force is calculated by multiplying the matrix of viscous damping $\mathbf{b}_\mathrm{vis}$ by the vector of velocity $\dot{\mathbf{X}}(t)$. Only the viscous damping in the heave direction is considered, and it is obtained through free decay tests performed in Star CCM+ [50]. The time domain wave excitation force $\mathbf{F}_\mathrm{wave}(t)$ can be calculated by the frequency domain wave excitation force $\mathbf{F}_\mathrm{wave}(\omega)$ and its phase angle $\boldsymbol{\varphi}_\mathrm{wave}(\omega)$ calculated by WAFDUT. A ramping function defined by Zhou *et al*. [51] and well applied by Jin *et al*. [52] is employed to keep the floats from a sudden large motion

$$R = \begin{cases} \frac{1}{2}\left[1 - \cos\frac{\pi t}{t_\mathrm{b}}\right], & (t < t_\mathrm{b}) \\ 1, & (t \geq t_\mathrm{b}) \end{cases} \tag{3}$$

where t_b is the baffling time. Each element of the time-domain wave excitation force is then

$$F_\mathrm{wave}(t) = R\left|F_\mathrm{wave}(\omega)\right|\cos\left[\omega t + \varphi_\mathrm{wave}(\omega)\right] \tag{4}$$

The PTO force is

$$\mathbf{F}_\mathrm{PTO}(t) = b_\mathrm{PTO} \cdot \dot{\mathbf{X}}(t) \tag{5}$$

where b_PTO is the linear PTO damping. The constraint force $\mathbf{F}_\mathrm{c}(t)$ can be transformed using the augment method with a Lagrange multiplier $\boldsymbol{\lambda}$ based on the multi-body dynamics [53]

$$\begin{bmatrix} \mathbf{M} + \mathbf{a}_\infty & \mathbf{C}_\mathrm{X}^\mathrm{T} \\ \mathbf{C}_\mathrm{X} & \mathbf{0} \end{bmatrix} \begin{bmatrix} \ddot{\mathbf{X}}(t) \\ \boldsymbol{\lambda} \end{bmatrix} = \begin{bmatrix} \mathbf{F}_\mathrm{ex}(\mathbf{X}, t) - \int_{-\infty}^{t} \kappa(t-\tau)\dot{\mathbf{X}}(t)\,d\tau - \mathbf{k}_\mathrm{r}\mathbf{X}(t) \\ \mathbf{F}_\mathrm{d}(t_0) \end{bmatrix} \tag{6}$$

The form of the constraint matrix $\mathbf{C}_\mathrm{X}$ can be referred to Zhou *et al*. [41]. By assuming the small-amplitude motion of the floats, the generalized force vector $\mathbf{F}_\mathrm{d}$ can be assigned the value at the initial time $t=t_0$. Then it has the same form as in the frequency-domain analysis by Zhou *et al*. [41]. The dynamic constraint equation of the hybrid system is solved at each instant, and the iteration of the displacement, velocity, and acceleration is accomplished by the fourth-order Ronge-Kutta method [54].

3.2 Wind and wave energy conversion

The instant wave power generated through the relative heave motion of the spar and the WEC is:

$$P_{\mathrm{wave}}\left(t\right)=\frac{1}{2}b_{\mathrm{PTO}}\left|\dot{z}_{\mathrm{Hywind}}\left(t\right)-\dot{z}_{\mathrm{WEC}}\left(t\right)\right|^{2} \tag{7}$$

where $\dot{z}_{\mathrm{Hywind}}(t)$ and $\dot{z}_{\mathrm{WEC}}(t)$ are the heaving velocities of the spar and the WEC, respectively.

3.3 Validation

The accuracy of the aero-servo module of OpenFAST and the multi-body hydrodynamics of WAFDUT has been extensively validated in previous works. The multi-body constraint dynamics in the in-house code have been validated by Zhou *et al*. [41]. Therefore, the validation in this study focuses on the coherence between the aero-servo module of OpenFAST and the hydrodynamics of the in-house code in the time domain.

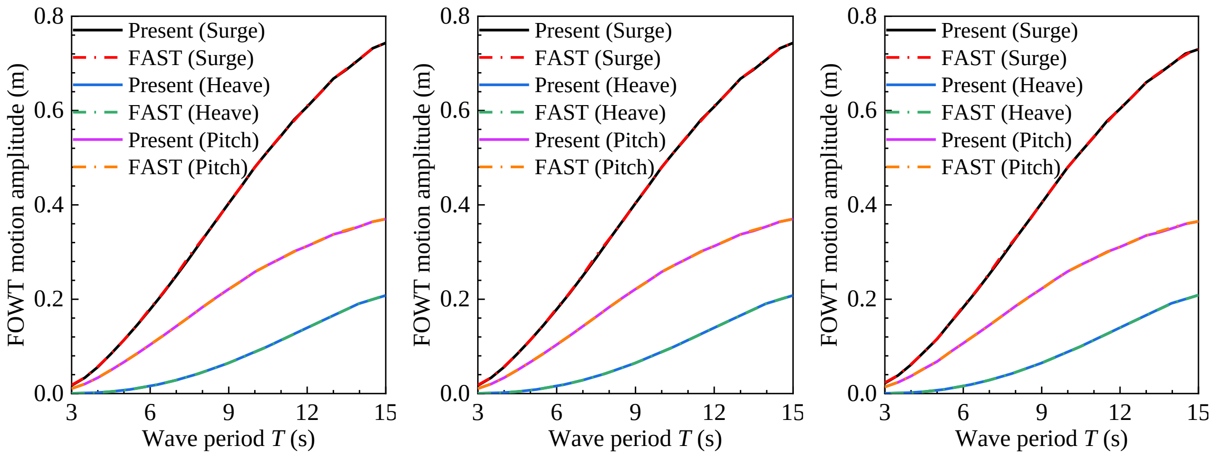

(a) U=8 m/s (b) U=11.4 m/s (c) U=15 m/s

Figure 3 Comparison of Hywind motions

Here a two-step validation process is performed through Hywind. It first demonstrates that the present hydrodynamic module works as well as the hydrodynamic module in OpenFAST. The surge, heave, and pitch motion amplitudes of Hywind in waves from 3 s to 15 s and three different wind speeds 8 m/s, 11.4 m/s (rated wind speed), and 15 m/s are calculated and compared. The results are shown in Figure 3. Good agreements are achieved with a maximum error of less than 0.1%. It then demonstrates that the aero-servo module of OpenFAST works well while it cooperates with the hydrodynamic module of either OpenFAST or the present in-house code. The wave period of T_p=8.54 s is used. Comparative results of the thrust force on the rotor and the generated wind power are shown in Figure 4. Good agreements are also achieved with a maximum error of less than 0.1%.

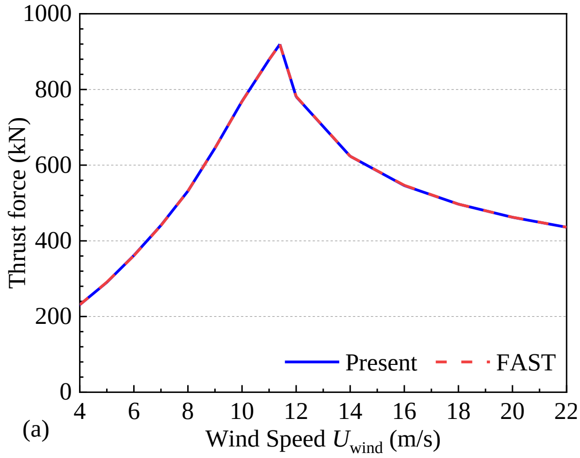

(a) Thrust force

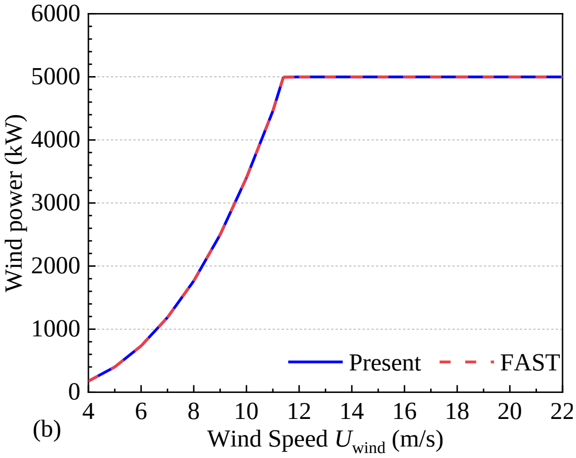

(b) Wind power

Figure 4 Comparisons of thrust force and wind power, T_{ave}=8.54 s

4. Coupled dynamic and power features of the hybrid system

The dynamic features, mooring loads, and energy conversion performance of the wind-wave hybrid system are analyzed in a wide range of wind and wave conditions. The results of an isolated Hywind are also proposed as a comparative reference to investigate the influence of the annular WEC. In these investigations, steady winds from U=3 m/s (cut-in speed) to U=25 m/s (cut-out speed) with an increment of 1 m/s and the wind with the rated speed of U=11.4 m/s are employed. Regular incident waves propagating in the positive-x direction with unit amplitude and the period from T=3 s to T=15 s with an increment of 0.5 s are employed. The water depth is 320 m.

4.1 Dynamic features

As the hybrid system is simulated in steady winds and linear regular waves, the motions of the Hywind in the surge, heave, and pitch directions are harmonic oscillations characterized by their equilibrium displacements and amplitudes. Results of equilibrium displacements and motion amplitudes are shown and interpreted. The maximum displacements are also shown to evaluate the stability of the system.

4.1.1 Equilibrium displacement

The equilibrium displacements of the Hywind platforms in the hybrid system, in isolation, and the difference between the two in the surge, heave, and pitch directions are shown in Figure 5~Figure 7, respectively. The rated wind speed U=11.4 m/s is marked by a white line. The same trend appears for the Hywind either in the hybrid system or in isolation in all three DoFs. As wind speed increases, the equilibrium displacement increases and decreases, reaching a peak at the rated wind speed. Compared with wind speed, wave period has a much smaller influence on the equilibrium displacement. These results indicate that the fundamental pattern of equilibrium displacement in different sea conditions is a property of Hywind dominated by wind speed and not affected by the annular WEC. A closer examination of the results reveals that the equilibrium displacement depends on the thrust force on the rotor (Figure 4a) as the two have nearly identical trends against wind speed. As the thrust force increases in the surge direction, its horizontal component increases and drifts the wind platform farther from its original position. In the pitch direction, the torque exerted by the thrust force increases and the tilted angle of the platform is enlarged by the increased torque. In the heave direction, the vertical component of the thrust force increases partly due to the increase in the thrust force itself and partly due to the increase in the titled angle of the platform. The increase of the vertical force presses the platform to a greater submergence depth, reflected by a greater draft.

In Figure 5c~Figure 7c, the difference between the Hywinds in the hybrid system and isolation shows that the equilibrium displacement in any of the three DoFs will be reduced by installing an annular WEC. In the pitch direction, the annular WEC increases the overall hydrostatic restoration stiffness of the hybrid system. The hybrid system needs to tilt with a smaller pitch angle to balance the torque exerted by the thrust force. The equilibrium displacement is therefore reduced. In the heave direction, the vertical component of the thrust force that presses the platform downward is diminished as the equilibrium tilted angle in the pitch direction decreases. The platform is then buoyed higher in the water, and its draft decreases. In the surge direction, the situation is a bit more complex. As the equilibrium angle in the pitch direction increases, it no longer needs that considerable mooring tension to balance the torque exerted by the thrust force to maintain the tilted equilibrium position. The total mooring tension is therefore reduced. As the draft of the platform is reduced, the vertical mooring tension is increased. As the total mooring tension is reduced and its vertical component is increased, its horizontal component, the mooring tension in the surge direction, is consequently reduced. It then no longer needs that long drift distance to tighten the cables to maintain that large horizontal mooring tension. The equilibrium displacement in the surge direction is then reduced.

The difference in the equilibrium displacement between the Hywind in the hybrid system and isolation is also dominated by wind conditions. Its peak value also occurs at the rated wind speed. Above all, the static stability of the Hywind depends on the wind condition, and it can be improved by combining it with an annular WEC. The improvements in the surge and pitch directions are more significant than that in the heave direction. Notably, improving static stability in the pitch direction can significantly promote the safety of Hywind.

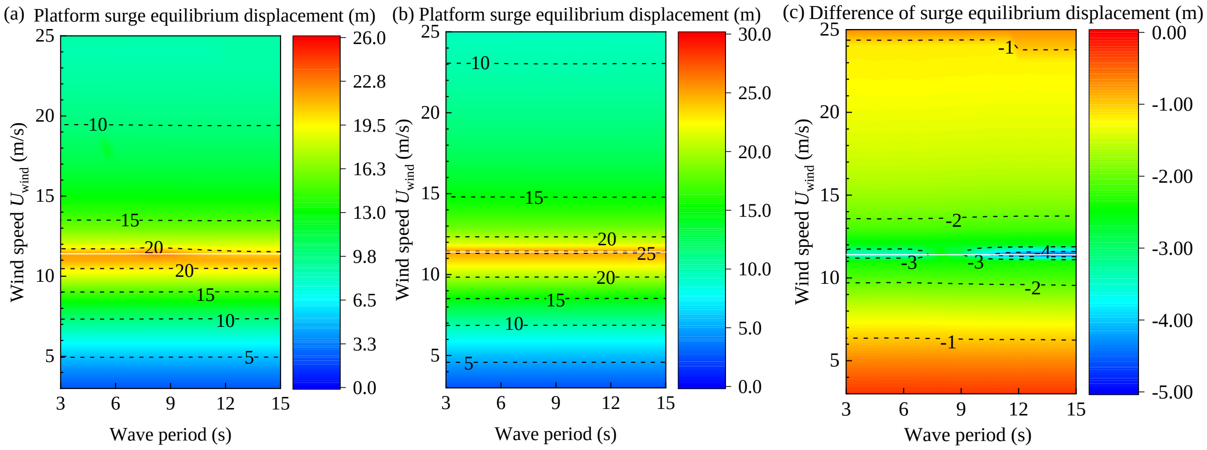

(a) Hybrid (b) Hywind (c) Difference (Hybrid−Hywind)

Figure 5 Equilibrium displacements of Hywind in surge direction

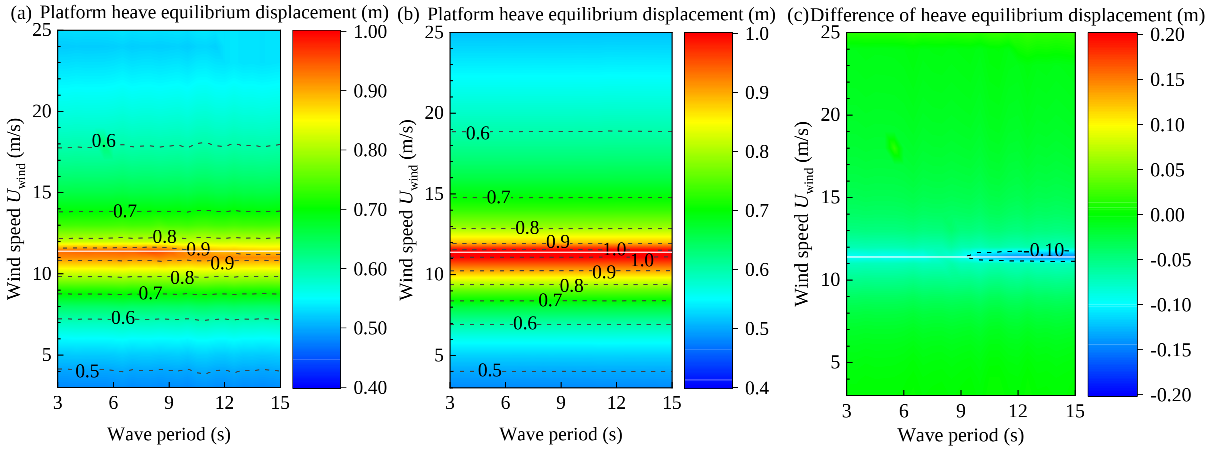

(a) Hybrid (b) Hywind (c) Difference (Hybrid−Hywind)

Figure 6 Equilibrium displacements of Hywind in heave direction

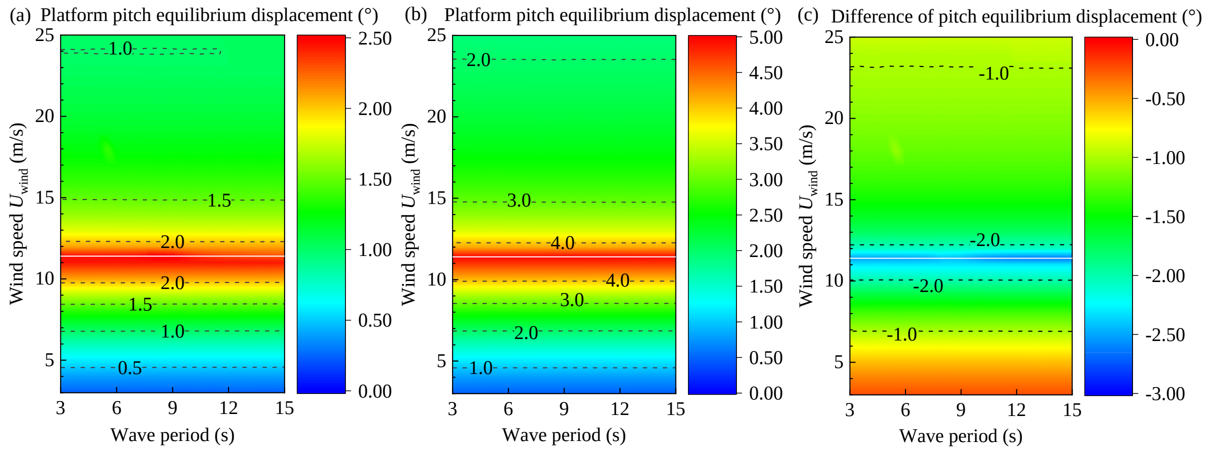

(a) Hybrid (b) Hywind (c) Difference (Hybrid−Hywind)

Figure 7 Equilibrium displacements of Hywind in the pitch direction

4.1.2 Motion amplitude

The motion amplitudes of the Hywind platforms in the hybrid system, in isolation, and the difference between the two in the surge, heave, and pitch directions are shown in Figure 8~Figure 10, respectively. In each DoF, the changing trends of motion amplitude of the Hywind in the hybrid system and isolation are nearly the same, but those in the surge and pitch directions are slightly different from that in the heave direction. The heave motion amplitude almost changes little for different wind speeds, increasing as the wave period increases. The fundamental pattern can be divided into two parts in the surge and pitch directions, separated by the rated wind speed. In either part with wind speed smaller or larger than the rated wind speed, the motion amplitude changes quite slightly against wind speed, which increases as the wave period increases. A sudden drop in motion amplitude occurs around the rated wind speed, and this phenomenon is more evident in long waves.

As shown in Figure 8c~Figure 10c, the difference in the motion amplitude is quite evenly distributed against the wind speed but changes largely against the wave period, indicating that the sudden drop is not caused by the annular WEC. The sudden declines in the surge and pitch motion amplitudes are caused by the servo system. As wind speed grows beyond the rated value, a switch of mode in the servo system changes the dynamic feature of Hywind, which triggers the sudden drop. The working principle of the servo system is to adjust the position of the wind turbine to make the rotor directly face the input wind. The servo system is sensitive to the surge and pitch motions of the platform as they affect the relative speed between the rotor and the input wind but is not sensitive to the heave motion. As the waves become longer, the wave forces increase and excite a larger motion, which exerts a greater influence on the servo system and intensifies the sudden drop.

The difference between the Hywinds in the hybrid system and isolation shows that the motion in any of the three DoFs will be increased by installing an annular WEC. The mechanism is quite simple in the surge and pitch directions. The annular WEC brings additional wave force, damping, and hydrostatic restoration stiffness in any of the three DoFs. A rigid connection passes the wave forces on the annular WEC to the wind platform. The increase in wave force will increase the motion amplitudes of the Hywind, whereas the increases in damping and hydrostatic restoration stiffness will reduce the motion amplitude. The results indicate that the increase in wave force exceeds the increases in damping and hydrostatic restoration stiffness, and the motion amplitude is consistently increased. As the surge motion of the hybrid system has a limited effect on the wave power generation using the relative heave motion, an extended active tuned mass damper [42] or tuned mass damper-nonlinear energy sink [43] can be employed to mitigate the WEC-induced increase in the surge motion amplitude. In the heave direction, the mechanism is a bit more complex as the presence of the PTO force constitutes an additional source of the force that intensifies the motion amplitude of Hywind. The difference in the motion amplitudes between the Hywind in the hybrid system and isolation is also dominated by wave conditions. Above all, the dynamic stability of the Hywind depends on wave conditions and is reduced by the annular WEC.

The reduction in the heave direction is greater than in the surge and pitch directions.

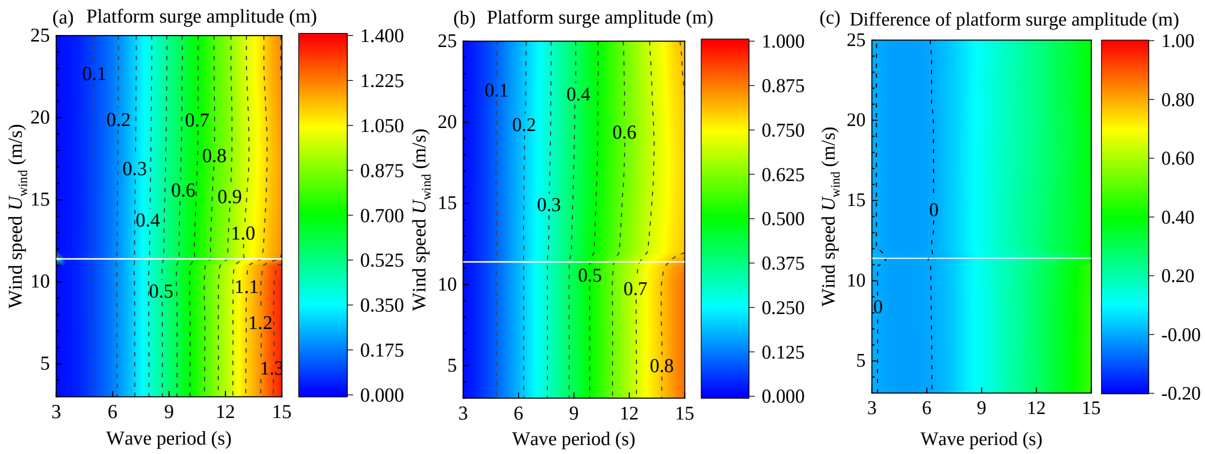

(a) Hybrid (b) Hywind (c) Difference (Hybrid−Hywind)

Figure 8 Motion amplitudes of Hywind in surge direction

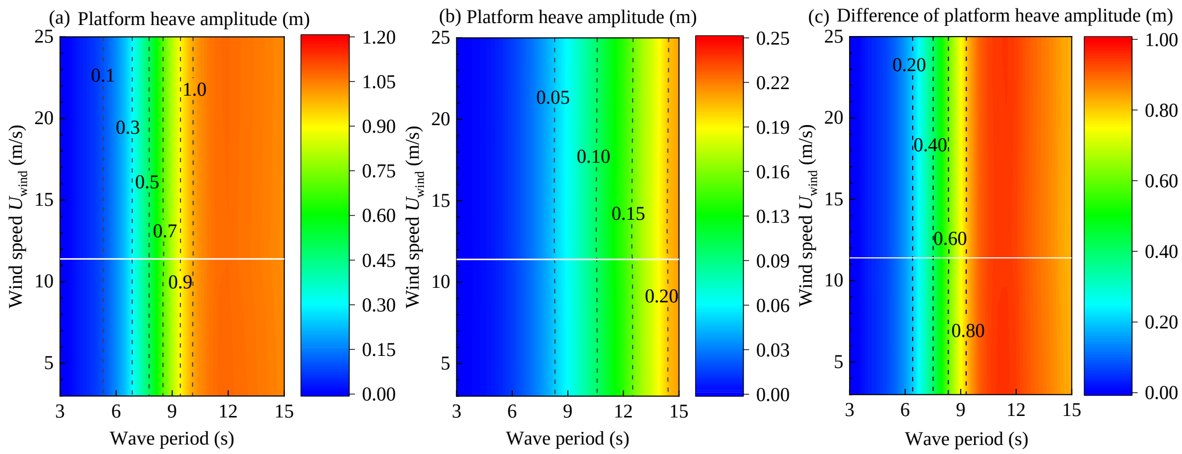

(a) Hybrid (b) Hywind (c) Difference (Hybrid−Hywind)

Figure 9 Motion amplitudes of Hywind in heave direction

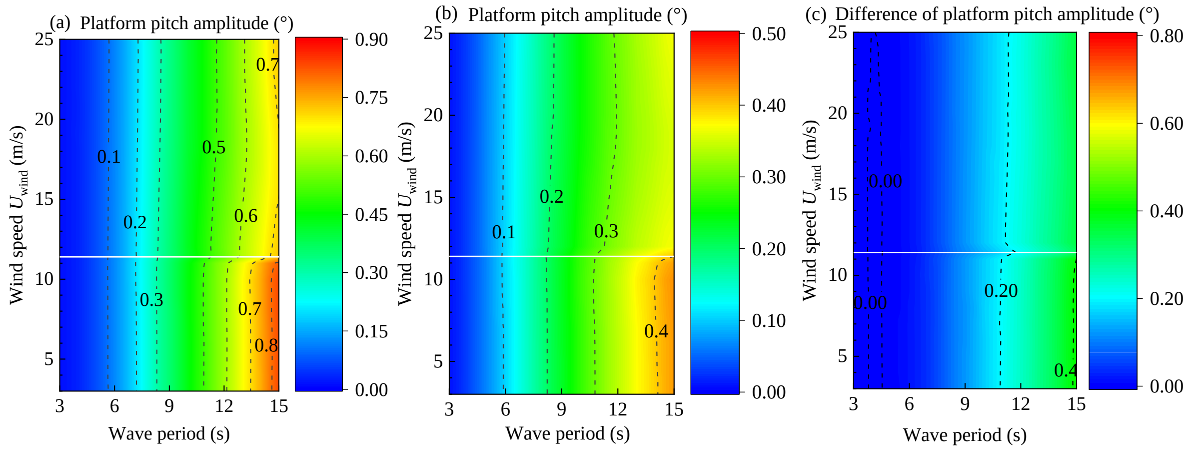

(a) Hybrid (b) Hywind (c) Difference (Hybrid−Hywind)

Figure 10 Motion amplitudes of Hywind in the pitch direction

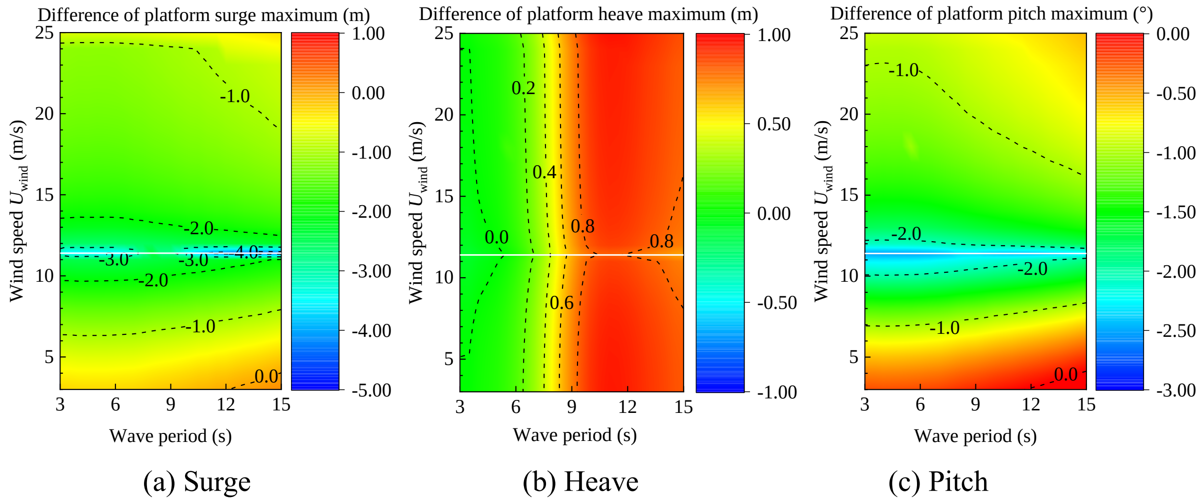

Figure 11 Difference of platform maximum displacements between hybrid system and Hywind

Figure 11 shows differences between the Hywinds in the hybrid system and isolation in the maximum displacements in the surge, heave, and pitch directions. Generally, the annular WEC reduces the maximum displacements of the Hywind in the surge and pitch direction and increases that in the heave direction. It improves the stability of the Hywind in the pitch direction, particularly around the rated wind speed. On the other hand, a compromise between the generation of wave power and the increase in the heave motion has to be made according to specific situations.

4.2 Maximum mooring tension

The maximum mooring tension on cable #1 and cable #2 (#3) of the hybrid system, the isolated Hywind, and their differences are shown in Figure 12 and Figure 13, respectively. The changing trends of the maximum mooring tensions are the same in the hybrid system and the isolated Hywind. It varies a lot as wind speed changes and varies relatively slightly against the wave period. These indicate that the fundamental patterns of the maximum mooring tensions in different sea conditions are the property of Hywind dominated by wind speed and not affected by the annular WEC. The maximum mooring tension on cable #1 (Figure 12) decreases and then increases, reaching a trough at the rated wind speed.

The maximum mooring tension on cable #2 (#3) (Figure 13) shows an opposite trend to cable #1. The opposite trends of maximum mooring tensions on cable #1 and cable #2 are caused by the spatial relationships between each fairlead and its corresponding anchor point. As evident by the dynamic features of the hybrid system in Section 4.1, the relative position between a fairlead and its corresponding anchor point is mainly determined by the equilibrium displacement of the Hywind in the surge direction. As wind speed increases from U=3 m/s to U=11.4 m/s, the Hywind moves toward the positive-x direction. The distance between the fairlead and its anchor point of cable #1 decreases, whereas that of cable #2 increases. The mooring tensions on the cables then change accordingly. As wind speed reaches U=11.4 m/s, the Hywind reaches its farthest equilibrium displacement in the surge direction, reflecting a trough of the maximum mooring tension on cable #1 and a peak of that on cable #2. As wind speed further increases, the Hywind moves back toward the negative-x direction. The maximum mooring tension on cable #1 increases and that on cable #2 decreases accordingly.

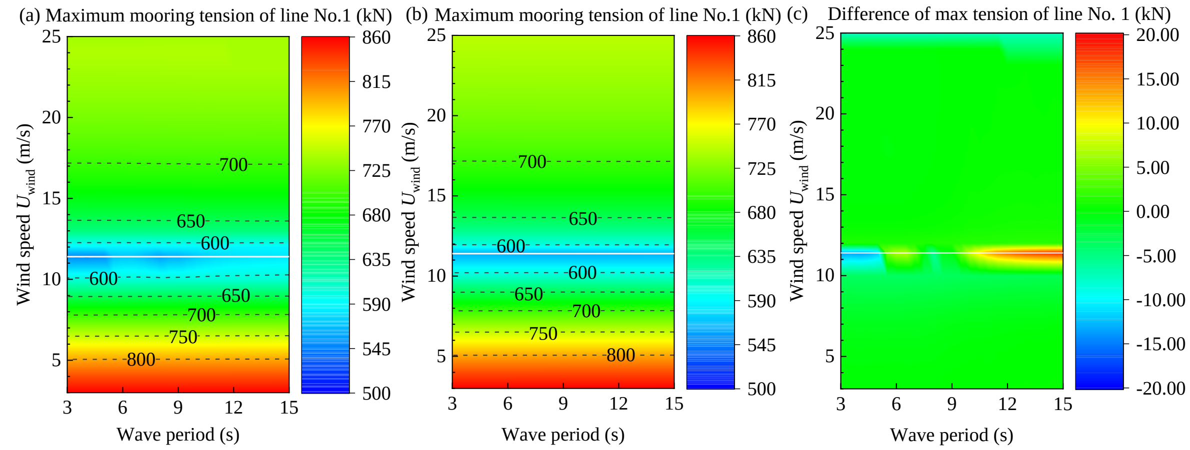

(a) Hybrid (b) Hywind (c) Difference (Hybrid−Hywind)

Figure 12 Maximum mooring force on cable #1 in different sea states

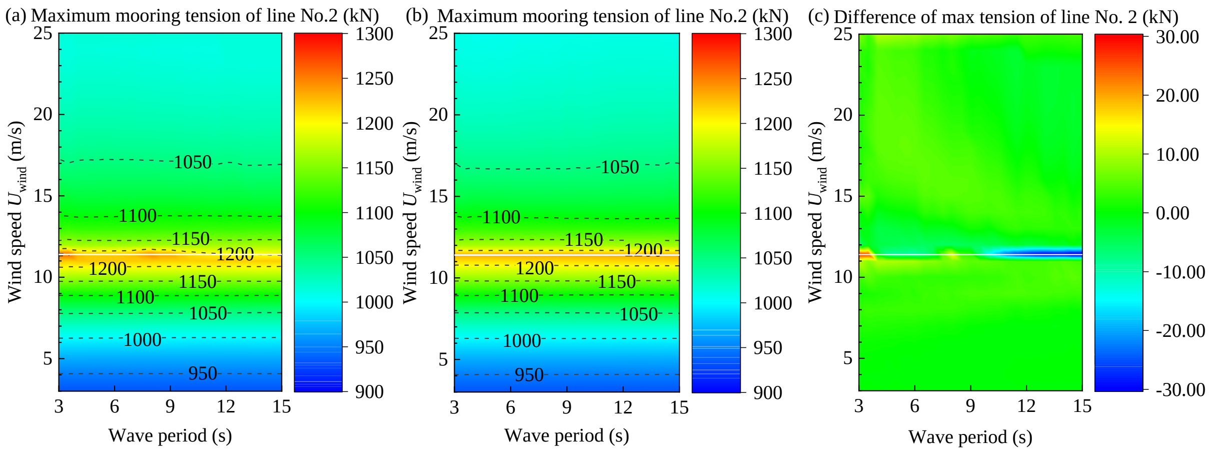

(a) Hybrid (b) Hywind (c) Difference (Hybrid−Hywind)

Figure 13 Maximum mooring force on cable #2 in different sea states

The overall changes in the maximum mooring tensions due to the annular WEC are pretty small compared with the magnitudes of their absolute values, from which it can be concluded that the annular WEC has quite limited influence on the mooring of the Hywind. Interestingly, however, a low-value region occurs in the maximum total mooring tension difference around the rated wind speed in long waves, revealed by Figure 12c and Figure 13c. This region is related to the area with a significant difference in the equilibrium displacement in the surge direction shown in Figure 5c. The annular WEC reduces the equilibrium displacement in the surge direction, which lead to an increase in the mooring tension on cable #1 and a decrease in the mooring tension on cable #2. Since cable #2 (#3) suffers the higher mooring tension and the decrease of mooring tension on cable #2 (#3) exceeds the increase of mooring tension on cable #1, the combined result is a reduction of the total mooring tension.

The maximum increase and decrease of the mooring tension of cable #1 and cable #2 (#3) are summarized in Table 6. With the addition of the annular WEC, the mooring tensions of cable #1 and cable #2 (#3) are at most increased by 3.14% and 2.20% whereas reduced by 2.48% and 2.87%, respectively. The maximum changes of the mooring tensions appear at the rated wind speed.

Table 6 The maximum increase and decrease of the mooring tension

Mooring line No.	Maximum increase/decrease	Sea state	
		Wave period	Wind speed
1	3.14%	15	11.4
2&3	2.20%	3	11.4
1	-2.48%	3	11.4
2&3	-2.87%	15	11.4

4.3 Mutual influence of energy conversion

This section investigates the mutual influence between the wind turbine and the annular wave energy converter on their transient wind and wave energy conversion performance. Figure 14 shows the wind power of the hybrid system, the isolated Hywind, and the difference between the two. The general trend of wind power in different sea states is not affected by the annular WEC. The wind power increases to its rate power 5 MW as wind speed increases to U=11.4 m/s and keeps approximately constant as wind speed further increases, which is the same as that shown in Figure 4b. The wind power distributes quite evenly against the wave period, indicating it is nearly unaffected by the wave condition.

Figure 14c shows that the annular WEC slightly improves the wind power while the wind is below the rated speed, particularly in shorter waves. This is because the annular WEC reduces the equilibrium tilted angle of the Hywind in the pitch direction, making the rotor face the input wind more directly. In the shorter waves, the motion amplitude in the pitch direction is smaller, which leads to a more stable increase in wind power. While wind is beyond the rated speed, the wind power reaches its upper limit and cannot be further improved by the annular WEC. Evidence can be found in the comparison between Figure 11c and Figure 14c, where the increase in wind power shows similar trends to that of the decrease of the platform displacement in the pitch direction.

Figure 15 shows the wave power of the hybrid system in different sea states. The mean peak period T_{ave}=8.54 s is marked by a white line. The wave power increases and then decreases, reaching a peak at 8.54 s, whereas it is nearly not affected by wind speed.

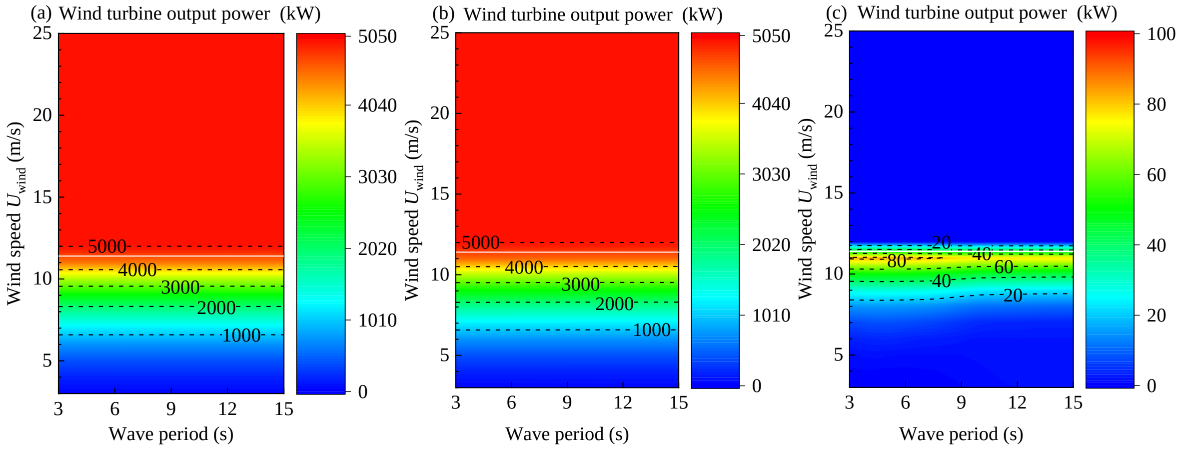

(a) Hybrid (b) Hywind (c) Difference (Hybrid−Hywind)

Figure 14 Wind turbine output power under different wind speeds and wave periods

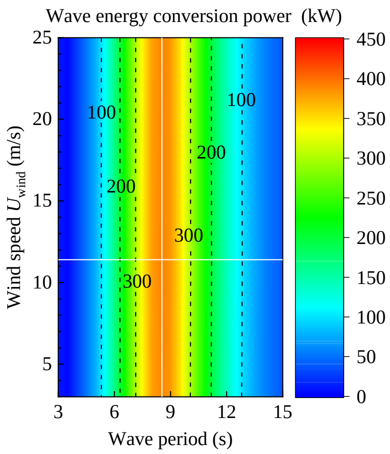

Figure 15 Wave power production of the hybrid system under different wave periods and wind speeds

5. Evaluation of wind and wave power in real sea states

The annual wind power and wave power of the hybrid system are evaluated based on the hindcast data at 59N3E in the North Sea provided by MetOceanView [44]. The annual wave and wind spectra are shown in Table 7 and Table 8, respectively. The mean peak wave period and wind speed are T_{ave}=8.54 s (ω_{ave}=0.753 rad/s) and U_{ave}=8.94 m/s, respectively. The mean peak wave period T_{ave} was also used in previous work [41] to obtain the optimized geometry and PTO damping of the annular WEC employed in this investigation. Taking the mean peak wave period as an example, it can be calculated by

$$T_{ave} = \sum_{j=1}^{17} \sum_{i=1}^{24} T_j S_{wave,ij} \tag{8}$$

where $S_{wave,ij}$ is the ijth occurrence probability given in Table 7 and T_j is the jth peak period calculated based on the data in Table 7. For instance, in the 3rd peak period interval, 4−5 s, T_3 is taken as 4.5 s.

The annual mean wind power and wave power are evaluated based on the following equations [55]:

$$P_{\text{wind}} = \sum_{i=1}^{12} \sum_{j=1}^{8} P_{\text{wind},ij} \times S_{\text{wind},ij} \tag{9}$$

$$P_{\text{wave}} = \sum_{i=1}^{24} \sum_{j=1}^{17} P_{\text{wave},ij} \times S_{\text{wave},ij} \tag{10}$$

where in $S_{\text{wind},ij}$ and $P_{\text{wind},ij}$ are the occurrence probability and mean wind power of the ith wind speed in the jth direction, respectively. $P_{\text{wave},ij}$ is the mean wave power of the ith wave height in the jth wave period, respectively.

Table 7 Annual wave occurrence probability at 59N3E in the North Sea (Unit: %)

Wave height H_i (m)	Peak period T_j (s)																
	2–3	3–4	4–5	5–6	6–7	7–8	8–9	9–10	10–11	11–12	12–13	13–14	14–15	15–16	16–17	17–18	18–19
0–0.5	0.0010	0.0342	0.0846	0.0257	0.0466	0.1264	0.0314	0.0342	0.0228	0.0038	0.0076	0.0105	0.0029	0	0	0.0029	0.0010
0.5–1	0.0019	0.1483	1.4065	2.1934	1.3172	2.3948	2.5545	0.7289	0.5883	0.3298	0.1967	0.1273	0.0637	0.0561	0.0143	0.0029	0.0010
1–1.5	0	0.0010	0.9950	4.5464	4.3601	3.4810	2.4138	1.1404	1.1718	0.9655	0.5493	0.4200	0.1283	0.0608	0.0105	0.0048	0.0029
1.5–2	0	0	0.0181	1.8769	4.1520	4.1995	2.5592	1.5975	0.7916	0.6605	0.5141	0.6130	0.1502	0.1112	0.0333	0.0057	0
2–2.5	0	0	0	0.1416	2.5288	4.2451	2.7597	1.9054	1.1537	0.4343	0.3041	0.4733	0.1635	0.1311	0.0181	0.0038	0
2.5–3	0	0	0	0.0010	0.4752	3.2397	3.0791	1.5471	1.2117	0.4771	0.1416	0.2765	0.0969	0.0988	0.0409	0.0124	0.0010
3–3.5	0	0	0	0	0.0200	1.3029	2.8947	1.5452	0.9256	0.5388	0.1368	0.1254	0.0646	0.0846	0.0247	0.0143	0.0048
3.5–4	0	0	0	0	0	0.2024	2.1772	1.6650	0.7032	0.4352	0.1473	0.0732	0.0361	0.0390	0.0190	0.0029	0.0048
4–4.5	0	0	0	0	0	0.0086	0.7584	1.8740	0.6595	0.3117	0.1663	0.0599	0.0295	0.0105	0.0114	0.0048	0
4.5–5	0	0	0	0	0	0	0.1606	1.4055	0.6861	0.2328	0.1036	0.0627	0.0162	0.0038	0.0038	0.0010	0
5–5.5	0	0	0	0	0	0	0.0124	0.5854	0.7584	0.2167	0.0855	0.0675	0.0086	0.0010	0.0010	0.0010	0
5.5–6	0	0	0	0	0	0	0	0.1587	0.7631	0.1796	0.0684	0.0475	0.0057	0.0010	0.0038	0.0010	0
6–6.5	0	0	0	0	0	0	0	0.0209	0.5540	0.1901	0.0618	0.0304	0.0038	0.0010	0	0.0010	0
6.5–7	0	0	0	0	0	0	0	0.0010	0.2252	0.2195	0.0418	0.0314	0.0019	0.0010	0	0	0
7–7.5	0	0	0	0	0	0	0	0	0.0656	0.2005	0.0333	0.0190	0.0057	0.0010	0	0	0
7.5–8	0	0	0	0	0	0	0	0	0.0114	0.1283	0.0390	0.0257	0.0038	0.0019	0	0	0
8–8.5	0	0	0	0	0	0	0	0	0	0.0808	0.0304	0.0152	0.0038	0	0	0	0
8.5–9	0	0	0	0	0	0	0	0	0	0.0181	0.0390	0.0124	0.0038	0	0	0	0
9–9.5	0	0	0	0	0	0	0	0	0	0.0019	0.0304	0.0095	0.0019	0	0	0	0
9.5–10	0	0	0	0	0	0	0	0	0	0	0.0095	0.0124	0.0019	0	0	0	0
10–10.5	0	0	0	0	0	0	0	0	0	0	0.0038	0.0086	0.0038	0.0010	0	0	0
10.5–11	0	0	0	0	0	0	0	0	0	0	0	0.0029	0.0019	0.0010	0	0	0
11–11.5	0	0	0	0	0	0	0	0	0	0	0	0.0029	0	0	0	0	0
11.5–12	0	0	0	0	0	0	0	0	0	0	0	0.0029	0.0010	0	0	0	0

The time history of wind power is calculated by the aero-servo module of OpenFAST. Here the influence of the wind direction on the wind power generation is not considered. The turbine is assumed to be able to generate the same amount of wind power under the same wind speed regardless of the wind direction. The time history of wave power is calculated by Eq. (7). As the hindcast data provided by MetOceanView are not joint wind-wave data, an additional input wind condition is needed while calculating the wind power and vice versa. Here the following setting is used. While calculating the wind power, the wave period is set as the mean peak wave period T_{ave}=8.54 s and the wave height is set as unit amplitude. While calculating the wave power, the wind speed is set as the mean wind speed U_{ave}=8.94 m/s. Note that it is the only occasion that the mean peak wave period T_{ave} and the mean wind speed U_{ave} are employed in this analysis. In these simulations, the input wave heights and wind speeds are treated by the same method applied to the wave period T_j as described above. For example, while calculating the wind power using the data in the 4th row in Table 8, the input wind speed in OpenFAST is taken as 17.5 knots (8.955 m/s). To make it clear, the key input parameters in the calculation of wind power and wave power are shown in Table 9. $P_{wind,ij}$ and $P_{wave,ij}$ are obtained by simulating the model for a long time and taking the mean values in 50 wave periods in the time histories using a self-made raw data processing code after the results are numerically stable.

Table 8 Annual wind occurrence probability at 59N3E in the North Sea (Unit: %)

Wind speed U_i (knots)	Direction: N	NE	E	SE	S	SW	W	NW
0-5	0.7479	0.6918	0.6196	0.6462	0.6662	0.7118	0.7137	0.7232
5-10	2.2076	1.5205	1.4245	1.7220	2.1515	2.1287	2.1743	2.4262
10-15	3.3822	1.2858	1.1461	2.3711	3.8327	3.3908	2.9508	3.4820
15-20	3.4953	0.7508	0.7375	2.7464	4.1396	3.4088	2.9527	3.2530
20-25	2.4376	0.2927	0.4067	2.6951	3.2169	2.8576	2.5307	2.2428
25-30	1.1318	0.0884	0.1701	2.3929	1.9577	1.9140	1.5680	1.2430
30-35	0.4514	0.0257	0.0950	1.6270	0.8781	0.9864	0.7555	0.5740
35-40	0.1102	0.0076	0.0295	0.8078	0.2937	0.3516	0.2651	0.2224
40-45	0.0352	0	0.0095	0.2803	0.0789	0.0732	0.0694	0.0675
45-50	0.0086	0	0.0019	0.0684	0.0048	0.0124	0.0143	0.0209
50-55	0.0029	0	0.0010	0.0048	0.0010	0.0029	0.0019	0.0095
55-60	0	0	0.0010	0	0	0	0	0.0019

Table 9 Key input parameters in the calculation of wind and wave power

Calculation term	Input parameters
Wind power	U_i, $S_{wind,ij}$, T_{ave}=8.54 m/s, H=1 m
Wave power	H_i, T_j, $S_{wave,ij}$, U_{ave}=8.94 m/s

The results of the hybrid system and the isolated Hywind are shown in Figure 16. Compared with the isolated Hywind (2422.41 kW), the wind power of the hybrid system (2446.13 kW) increases by 0.98%. The wave power comprises 24.17% of the total power, constituting a considerable proportion. This indicates that wave power can be an effective supplement to wind power. Note that these results only indicate that integrating the annular WEC on the Hywind can improve the wind power and bring considerable extra power through a fine tune of the WEC parameters. The specific values of the improvement of wind power, 0.98%, and the proportion of wave power, 24.17%, obtained by this hybrid system in a selected operation site at 59N3E in the North Sea may not be over-generalized to other wind hybrid systems under a different operating condition. A higher or lower improvement may be obtained.

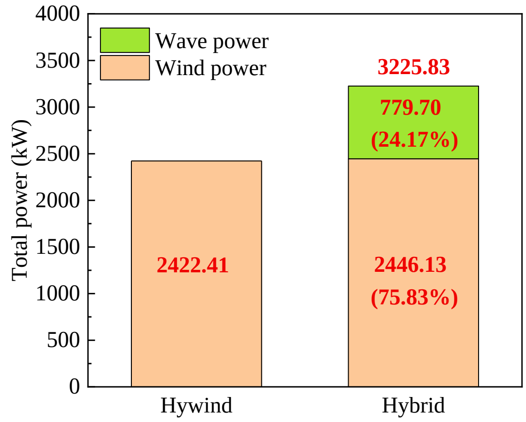

Figure 16 Annual power of isolated Hywind and hybrid system

6. Conclusion

This study proposes a numerical tool that can handle the full couplings in a complex multi-floating body wind-wave hybrid system and accurately predict the performance of the system. The numerical tool is used to analyze and evaluate the performance of a spar-type Hywind offshore wind turbine and an annular WEC hybrid system in a wide range of operating conditions, with varying wind speeds and wave periods. The dynamic features, mooring loads, and energy conversion performance of the hybrid system are investigated. Comparisons between the hybrid system and an isolated Hywind are also carried out to reveal the influence of the annular WEC. The major conclusions are as follows.

(1) The fundamental pattern of the static stability of the hybrid system in different sea states depends on wind speed (strictly speaking, the thrust force on the rotor) and is not affected by the annular WEC. The fundamental pattern of the dynamic stability depends on the wave period and is slightly modified by a switch of mode in the servo system and is also not affected by the annular WEC. The annular WEC can improve the static stability of the Hywind, particularly in the surge and pitch directions, but reduce the dynamic stability, particularly in the heave direction. The overall stability in the pitch direction is improved by the annular WEC. However, the designer has to compromise between the generation of wave power and the increase in the heave motion amplitude according to specific situations.

(2) The fundamental pattern of the maximum mooring tensions in different sea states depends on wind speed. In most situations, the maximum mooring tensions are reduced by the annular WEC, but its effect is so small that can be almost neglected.

(3) The annular WEC can improve the wind power of the hybrid system by reducing the tilted angle of the Hywind in the pitch direction. The energy conversion performance of the present hybrid system is evaluated based on the hindcast sea state in a randomly chosen target operation site at 59N3E in the North Sea. Wave power can account for about one-fourth of the total power, which is a large proportion and proved an effective supplement to wind power.

The present numerical tool can be further used to simulate and evaluate similar wind-wave hybrid systems. This study also provides knowledge about the key properties of the coupled dynamic and power generation features of the hybrid system. These findings can offer valuable insights and useful guidance for the practical design of wind-wave hybrid systems to improve performance and efficiency.

The limitations of this study are: 1) The investigation is based on numerical simulation in regular waves and steady winds. It does not consider all physical phenomena that may occur in real-world wind-wave hybrid systems. 2) The analysis is based on a specific hybrid system optimized according to specific wave conditions at a selected operation site. The results may not be generalizable to other hybrid systems or operating conditions.

Future works can be carried out in the following avenues: 1) The impact of the annular WEC on the dynamic stability of the hybrid system by performing sensitivity analyses on different design parameters. 2) The performance of the hybrid system in more complex sea states involving irregular, nonlinear waves and unsteady wind.

Acknowledgement

This work is supported by the National Natural Science Foundation of China (52071096, 52201322, and 52222109), Guangdong Basic and Applied Basic Research Foundation (2022B1515020036 and 2023A1515012144), and Fundamental Research Funds for the Central Universities (2022ZYGXZR014).

Reference

[1] López M, Rodríguez N, Iglesias G. Combined floating offshore wind and solar PV. *Journal of Marine Science and Engineering*. 2020 Jul 30;8(8):576.

[2] Fan, Y., Mu, A., & Ma, T. (2016). Modeling and control of a hybrid wind-tidal turbine with hydraulic accumulator. *Energy*, 112, 188-199.

[3] Pérez-Collazo, C., Greaves, D., & Iglesias, G. (2015). A review of combined wave and offshore wind energy. *Renewable and Sustainable Energy Reviews*, 42, 141-153.

[4] Astariz, S., & Iglesias, G. (2016). Co-located wind and wave energy farms: Uniformly distributed arrays. *Energy*, 113, 497-508.

[5] Gaughan, E., & Fitzgerald, B. (2020). An assessment of the potential for Co-located offshore wind and wave farms in Ireland. *Energy*, 200, 117526.

[6] Seventh Framework Programme of the European Community for research and technological development including demonstration activities (FP7). https://cordis.europa.eu/programme/id/FP7.

[7] Jeffrey, H., & Sedgwick, J. (2011). ORECCA European offshore renewable energy roadmap.

[8] Platform, M. A. R. I. N. A. European Union Seventh Framework Programme (EU FP7) Marine Renewable Integrated Application Platform (MARINA Platform).

[9] Kamarlouei, M., Gaspar, J. F., Calvario, M., Hallak, T. S., Mendes, M. J., Thiebaut, F., & Soares, C. G. (2020). Experimental analysis of wave energy converters concentrically attached on a floating offshore platform. *Renewable Energy*, 152, 1171-1185.

[10] Gaspar, J. F., Kamarlouei, M., Thiebaut, F., & Soares, C. G. (2021). Compensation of a hybrid platform dynamics using wave energy converters in different sea state conditions. *Renewable Energy*, 177, 871-883.

[11] Si, Y., Chen, Z., Zeng, W., Sun, J., Zhang, D., Ma, X., & Qian, P. (2021). The influence of power-take-off control on the dynamic response and power output of combined semi-submersible floating wind turbine and point-absorber wave energy converters. *Ocean Engineering*, 227, 108835.

[12] Zhou, B., Hu, J., Jin, P., Sun, K., Li, Y., & Ning, D. (2023). Power performance and motion response of a floating wind platform and multiple heaving wave energy converters hybrid system. *Energy*, 265, 126314.

[13] Ghafari, H. R., Ghassemi, H., & He, G. (2021). Numerical study of the Wavestar wave energy converter with multi-point-absorber around DeepCwind semisubmersible floating platform. *Ocean Engineering*, 232, 109177.

[14] Balat, M. (2009). A review of modern wind turbine technology. *Energy Sources*, Part A, 31(17), 1561-1572.

[15] Wu, X., Hu, Y., Li, Y., Yang, J., Duan, L., Wang, T., ... & Liao, S. (2019). Foundations of offshore wind turbines: A review. *Renewable and Sustainable Energy Reviews*, 104, 379-393.

[16] Drew, B., Plummer, A. R., & Sahinkaya, M. N. (2009). A review of wave energy converter technology.

[17] Falcão, A. F., & Henriques, J. C. (2016). Oscillating-water-column wave energy converters and air turbines: A review. *Renewable Energy*, 85, 1391-1424.

[18] Wan, L., Ren, N., & Zhang, P. (2020). Numerical investigation on the dynamic responses of three integrated concepts of offshore wind and wave energy converter. *Ocean Engineering*, 217, 107896.

[19] Muliawan, M. J., Karimirad, M., & Moan, T. (2013). Dynamic response and power performance of a combined spar-type floating wind turbine and coaxial floating wave energy converter. *Renewable Energy*, 50, 47-57.

[20] Wan, L., Gao, Z., & Moan, T. (2015). Experimental and numerical study of hydrodynamic responses of a combined wind and wave energy converter concept in survival modes. *Coastal Engineering*, 104, 151-169.

[21] Wan, L., Greco, M., Lugni, C., Gao, Z., & Moan, T. (2017). A combined wind and wave energy-converter concept in survival mode: Numerical and experimental study in regular waves with a focus on water entry and exit. *Applied Ocean Research*, 63, 200-216.

[22] Wan, L., Gao, Z., Moan, T., & Lugni, C. (2016). Comparative experimental study of the

survivability of a combined wind and wave energy converter in two testing facilities. *Ocean Engineering*, 111, 82-94.

[23] Wan, L., Gao, Z., Moan, T., & Lugni, C. (2016). Experimental and numerical comparisons of hydrodynamic responses for a combined wind and wave energy converter concept under operating conditions. *Renewable Energy*, 93, 87-100.

[24] Muliawan, M. J., Karimirad, M., Gao, Z., & Moan, T. (2013). Extreme responses of a combined spar-type floating wind turbine and floating wave energy converter (STC) system with survival modes. *Ocean Engineering*, 65, 71-82.

[25] Cheng, Z., Wen, T. R., Ong, M. C., & Wang, K. (2019). Power performance and dynamic responses of a combined floating vertical axis wind turbine and wave energy converter concept. *Energy*, 171, 190-204.

[26] Muliawan, M. J., Karimirad, M., Moan, T., & Gao, Z. (2012, July). STC (Spar-Torus Combination): a combined spar-type floating wind turbine and large point absorber floating wave energy converter—promising and challenging. In *International Conference on Offshore Mechanics and Arctic Engineering* (Vol. 44946, pp. 667-676). American Society of Mechanical Engineers.

[27] Faiz, J., & Nematsaberi, A. (2017). Linear electrical generator topologies for direct-drive marine wave energy conversion-an overview. *IET Renewable Power Generation*, 11(9), 1163-1176.

[28] Jin, P., Zhou, B., Göteman, M., Chen, Z., & Zhang, L. (2019). Performance optimization of a coaxial-cylinder wave energy converter. *Energy*, 174, 450-459.

[29] Fan, Y., Mu, A., & Ma, T. (2016). Design and control of a point absorber wave energy converter with an open loop hydraulic transmission. *Energy Conversion and Management*, 121, 13-21.

[30] Mu, A., Huang, Z., Liu, A., Wang, J., Yang, B., & Qian, Y. (2022). Optimal model reference adaptive control of spar-type floating wind turbine based on simulated annealing algorithm. *Ocean Engineering*, 255, 111474.

[31] Jaya Muliawan, M., Gao, Z., Moan, T., & Babarit, A. (2013). Analysis of a two-body floating wave energy converter with particular focus on the effects of power take-off and mooring systems on energy capture. Journal of Offshore Mechanics and Arctic Engineering, 135(3).

[32] Jonkman, J. (2010). Definition of the Floating System for Phase IV of OC3 (No. NREL/TP-500-47535). National Renewable Energy Lab. (NREL), Golden, CO (United States).

[33] Wang, Y., Zhang, L., Michailides, C., Wan, L., & Shi, W. (2020). Hydrodynamic response of a combined wind–wave marine energy structure. *Journal of Marine Science and Engineering*, 8(4), 253.

[34] Zhao, C., Thies, P. R., Ye, Q., & Lars, J. (2021). System integration and coupled effects of an OWT/WEC device. *Ocean Engineering*, 220, 108405.

[35] Yde, A., Pedersen, M. M., Bellew, S. B., Køhler, A., Clausen, R. S., & Wedel Nielsen, A. (2014).

Experimental and Theoretical Analysis of a Combined Floating Wave and Wind Energy Conversion Platform. DTU Wind Energy E No. 0044.

[36] Ren, N., Ma, Z., Shan, B., Ning, D., & Ou, J. (2020). Experimental and numerical study of dynamic responses of a new combined TLP type floating wind turbine and a wave energy converter under operating conditions. *Renewable Energy*, 151, 966-974.

[37] Karimirad, M., & Koushan, K. (2016, November). WindWEC: Combining wind and wave energy inspired by hywind and wavestar. I*n 2016 IEEE International Conference on Renewable Energy Research and Applications* (ICRERA) (pp. 96-101). IEEE.

[38] Michailides, C., Gao, Z., & Moan, T. (2016). Experimental study of the functionality of a semi-submersible wind turbine combined with flap-type Wave Energy Converters. *Renewable Energy*, 93, 675-690.

[39] Gao, Z., Moan, T., Wan, L., & Michailides, C. (2016). Comparative numerical and experimental study of two combined wind and wave energy concepts. *Journal of Ocean Engineering and Science*, 1(1), 36-51.

[40] Karimirad, M., & Moan, T. (2012). Wave-and wind-induced dynamic response of a spar-type offshore wind turbine. *Journal of Waterway, Port, Coastal, and Ocean Engineering*, 138(1), 9-20.

[41] Zhou B., Zheng Z., Wang Y., Jin P., Cui L., & Cheng L. (2023). Optimization of an annular wave energy converter in a wind-wave hybrid system. *Journal of Hydrodynamics*. (accepted).

[42] Mu, A., Huang, Z., Hu, J., Yang, B., Wang, J., Qian, Y., ... & Li, N. (2023). Research and numerical analysis of floating offshore wind turbine based on a novel extended tuned mass damper. *Physics of Fluids*, 35(3), 035108.

[43] Mu, A., Huang, Z., Hu, J., Yang, B., Wang, J., & Qian, Y. (2022). Stability analysis of floating wind turbine structure with turned mass damper-nonlinear energy sink. *Journal of Renewable and Sustainable Energy*, 14(3), 033302.

[44] MetOceanView. http://app.metoceanview.com/hindcast/sites/nsea/59/3#.

[45] Jonkman, J. M., & Buhl, M. L. (2005). FAST user's guide (Vol. 365, p. 366). Golden, CO, USA: National Renewable Energy Laboratory.

[46] Jonkman, J. M. (2007). Dynamics modeling and loads analysis of an offshore floating wind turbine. University of Colorado at Boulder.

[47] Cummins, W. E. (1962). The impulse response function and ship motions. David Taylor Model Basin Washington DC.

[48] Teng, B., & Taylor, R. E. (1995). New higher-order boundary element methods for wave diffraction/radiation. *Applied Ocean Research*, 17(2), 71-77.

[49] Liu, Y. (2015). A Coupled Approach for Dynamic Modelling of a Semi-submersible Type Platform with Multiple Diffuser-Augmented Wind Turbines (Doctoral dissertation, Kyushu University).

[50] CD-Adapco, S. (2017). STAR CCM+ user guide version 12.04. CD-Adapco: New York, NY, USA, 62.

[51] Zhou, B. Z., Ning, D. Z., Teng, B., & Bai, W. (2013). Numerical investigation of wave radiation by a vertical cylinder using a fully nonlinear HOBEM. *Ocean Engineering*, 70, 1-13.

[52] Jin, P., Zhou, B., Zhang, H., Chen, L., & Zhang, L. (2019). Ringing of the roll motion of a two-dimensional barge in focused wave groups. *Journal of Marine Science and Technology*, 24, 1029-1042.

[53] Shabana, A. A. (2020). Dynamics of multi-body systems. *Cambridge University Press*.

[54] Zhou, B. Z., Ning, D. Z., Teng, B., & Bai, W. (2013). Numerical investigation of wave radiation by a vertical cylinder using a fully nonlinear HOBEM. *Ocean Engineering*, 70, 1-13.

[55] Zhang, H., Zhou, B., Zang, J., Vogel, C., Jin, P., & Ning, D. (2021). Optimization of a three-dimensional hybrid system combining a floating breakwater and a wave energy converter array. *Energy Conversion and Management*, 247, 114717.